

Synergistic Multimodal Cancer Therapy Using Glucose Oxidase@CuS Nanocomposites

Parbeen Singh,[#] Brian Youden,[#] Yikun Yang, Yongli Chen, Andrew Carrier, Shufen Cui, Ken Oakes, Mark Servos, Runqing Jiang,* and Xu Zhang*



Cite This: <https://doi.org/10.1021/acsami.1c12235>



Read Online

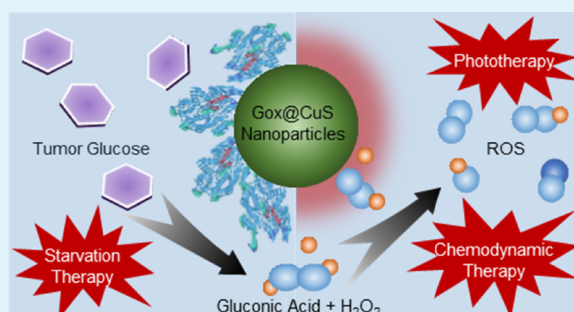
ACCESS |

Metrics & More

Article Recommendations

Supporting Information

ABSTRACT: Multimodal nanotherapeutic cancer treatments are widely studied but are often limited by their costly and complex syntheses that are not easily scaled up. Herein, a simple formulation of glucose-oxidase-coated CuS nanoparticles was demonstrated to be highly effective for melanoma treatment, acting through a synergistic combination of glucose starvation, photothermal therapy, and synergistic advanced chemodynamic therapy enabled by near-infrared irradiation coupled with Fenton-like reactions that were enhanced by endogenous chloride.



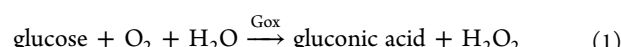
KEYWORDS: copper sulfide nanoparticles, glucose oxidase, Fenton reaction, cancer therapy, starvation therapy

1. INTRODUCTION

Cancer is a family of complex and dynamic diseases that evolves as it progresses.^{1,2} Therefore, effective monomodal treatment is challenging because of cellular heterogeneity, rapid metastasis, and the strong possibility of developing resistance to therapeutics. However, these challenges can be addressed through multimodal synergistic therapies that employ combinations of treatments.³ Combination therapies are ideal as they can maximize treatment efficacy while minimizing adverse side effects. Among these treatments, glucose oxidase (Gox)-based catalytic nanomedicine has emerged as an excellent technical platform for powerful multimodal cancer therapies.^{4–7}

An important hallmark of most cancerous cells is an increase in glucose uptake.⁸ Unlike normal cells, which often rely on mitochondrial oxidative phosphorylation to obtain energy, cancerous cells exhibit a preference toward aerobic glycolysis to drive their proliferation.⁹ However, this process is much less efficient at generating ATP overall and thus requires higher levels of glucose to meet the same energy demands. Gox catalyzes glucose oxidation using molecular oxygen to form gluconic acid and hydrogen peroxide (H_2O_2) (eq 1). Gox can therefore suppress tumor growth by depleting glucose, i.e., cancer starvation therapy (ST).^{10,11} This also lowers the local pH of tumor sites and generates H_2O_2 , which not only is toxic by itself to tumor cells but also serves as a precursor to generate even more toxic reactive oxygen, chlorine, and nitrogen species (reactive oxygen species (ROS), RCS, and RNS), e.g., singlet oxygen (1O_2),^{12,13} hydroxyl radicals ($^{\bullet}OH$),¹⁴ hypochlorous acid (HOCl),¹⁵ and nitric oxide

(NO),¹⁶ through Fenton-like reactions. These reactive species can kill tumor cells more efficiently than H_2O_2 . Therefore, as recently reviewed by Wang et al., combining Gox with a nanocatalyst to form a catalytic nanomedicine formulation that accelerates H_2O_2 decomposition for reactive species generation may present an effective multimodal synergistic cancer treatment.¹⁷



Compared to conventional chemotherapeutics, catalytic nanomedicine may be better tolerated by patients because the constituting therapeutic agents (Gox and nanocatalyst) are not toxic until combined. Thereafter, powerful short-lived reactive species are generated *in situ* to attack tumor cells in the tumor microenvironment (TME), which minimizes systemic toxicity while remaining effective in the tumor sites. Thus far, catalysts used in combination with Gox are either encapsulated enzymes, e.g., chloroperoxidase, catalase,¹⁸ and peroxidase,¹⁹ or catalytic nanoparticles (NPs), e.g., Fe_3O_4 NPs,^{20,21} amorphous Fe NPs, single-atom Fe nanocatalysts,^{22,23} porous hollow Prussian blue NPs,²⁴ Mn-doped $Ca_3(PO_4)_2$ NPs,²⁵ Ag NPs,²⁶ Pt NPs,²⁷ MnO_2 NPs,²⁸ Fe_5C_2

Received: June 29, 2021

Accepted: August 19, 2021

Scheme 1. Catalytic Therapeutic Mechanisms of Gox@CuS NPs for the Generation of Lethal ROS and Glucose Depletion for Tumor Therapy

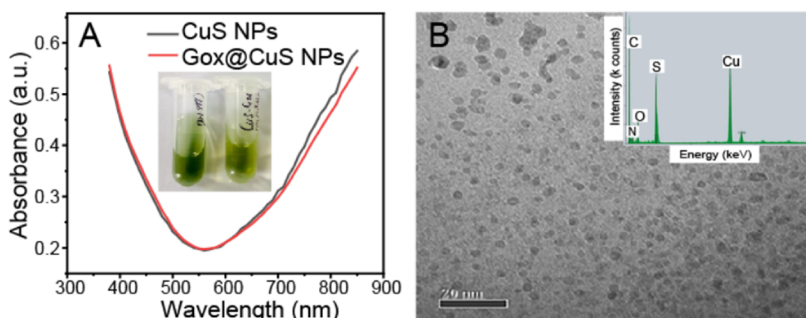
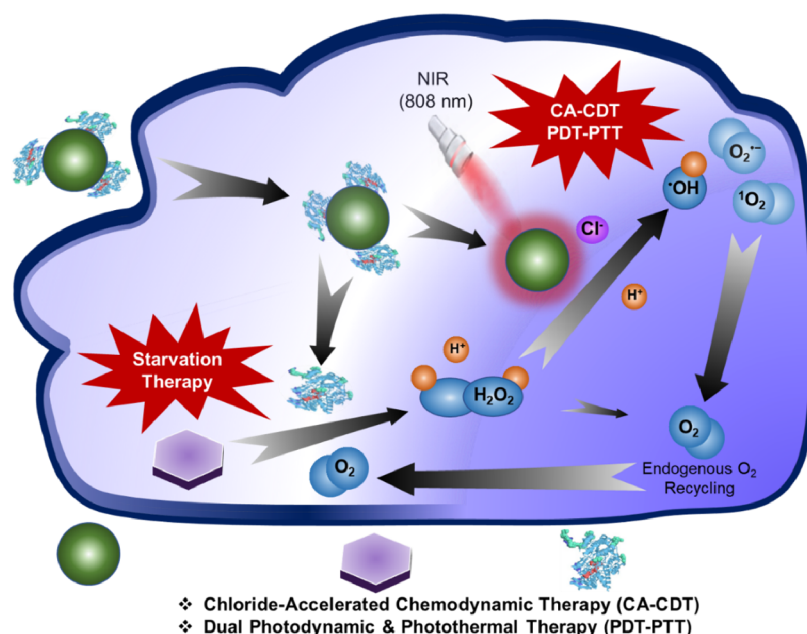


Figure 1. Characterization of CuS and Gox@CuS nanoparticles (NPs). (A) UV-vis spectra of CuS and Gox@CuS NPs. Inset: Photograph of the NP solutions. (B) TEM of Gox@CuS NPs showing an ultrasmall particle size (scale bar = 20 nm). Inset: EDX spectrum of the Gox@CuS NPs.

NPs,²⁹ etc. (more examples are given in Table S2). Although these catalysts are effective cancer therapeutics, they have technical and economic concerns, e.g., complex material synthesis and high cost, which hinder their translation to large-scale clinical applications.

Copper sulfide nanoparticles (CuS NPs) are an emerging theranostic platform that has great translational potential because of their excellent photothermal properties;³⁰ consistent near-infrared (NIR) absorption from the d-d energy transition of Cu²⁺ ions that is independent of the NP size, shape, and surrounding environment; low toxicity; biodegradability; and scalable and cost-effective synthesis.³¹ CuS NPs are promising low-temperature photothermal and photodynamic therapeutics,³² excellent contrast agents for photoacoustic and magnetic resonance imaging,^{30,33} and promising radiotherapy sensitizers.³⁴ Recently, our group discovered that chloride ions accelerate Cu-based Fenton chemistry (Cl–Cu Fenton),³⁵ generating reactive species including hydroxyl and chlorine radicals and singlet oxygen.^{12,36,37} This effect was observed for both Cu ions and CuO NPs, and the effect of chloride on ROS production has been further investigated in other systems with differing results.^{38–40} We hypothesize that chloride-accelerated Cu-Fenton may also apply to the catalytic activity of CuS NPs

in the tumor sites, especially when Gox is introduced simultaneously to produce H₂O₂ in situ. In addition, because NIR irradiation can generate electron–hole pairs⁴¹ and the Cu-Fenton reaction rate increases with temperature,⁴² we believe that the photothermal effect from NIR irradiation of CuS NPs will enhance radical generation, resulting in a more effective and efficient treatment (Scheme 1). In this work, we validated these hypotheses, resulting in a very simple, safe, and highly effective novel nanoformulation, i.e., Gox-coated CuS nanocomposites (Gox@CuS) that integrate cancer starvation therapy (ST), Cl-accelerated CuS-Fenton-based chemodynamic therapy (CA-CDT), and dual photothermal-photodynamic therapy (PTT-PDT) into a simple nanoplateform.

2. RESULTS AND DISCUSSION

The synthesized CuS NPs were spherical with an average size of 8 ± 2 nm (Figures S1 and 1B) as measured by transmission electron microscopy (TEM) and dynamic light scattering (DLS). The citrate capping ligand yielded a negative surface charge ($\xi = -28$ mV, Figure S2), but displacement by Gox conjugation greatly reduced this ($\xi = -2$ mV). Gox conjugation also increased the hydrodynamic size up to 13 ± 3 nm (Figure S3) and was further supported by FTIR (Figure

S4) and energy-dispersive X-ray (EDX) spectroscopy, which showed increased C, N, and O signals from the protein together with Cu and S (inset in Figure 1B and Table S1). As Cu²⁺ ions can be detected using a highly sensitive colorimetric assay based on the Cu–Cl Fenton reaction (Figure S5A), the concentration of the CuS NPs was determined by measuring the free Cu²⁺ left over from the NP synthesis via the standard addition calibration method.³⁵ Approximately 73% of free Cu was consumed during particle synthesis, and the Bradford assay indicated a high loading capacity of the CuS NPs (0.61 g of Gox per g of CuS, Figure S6), likely owing to the formation of disulfide bonds between the comparably sized particle and enzyme. Importantly, Gox adsorption did not significantly change the NIR absorption ($\lambda > 800$ nm) of the plasmonic CuS NPs (Figure 1A), which is responsible for their strong photothermal effect (Figure S7).

The Fenton activity of the CuS and Gox@CuS NPs was examined by monitoring the oxidation of the chromogenic substrate 2,2-azino-bis(3-ethylbenzothiazoline-6-sulfonate) (ABTS, $\lambda = 420$ nm) by ROS in the presence or absence of H₂O₂ and Cl⁻ (Figures 2A and S8). As previously observed by

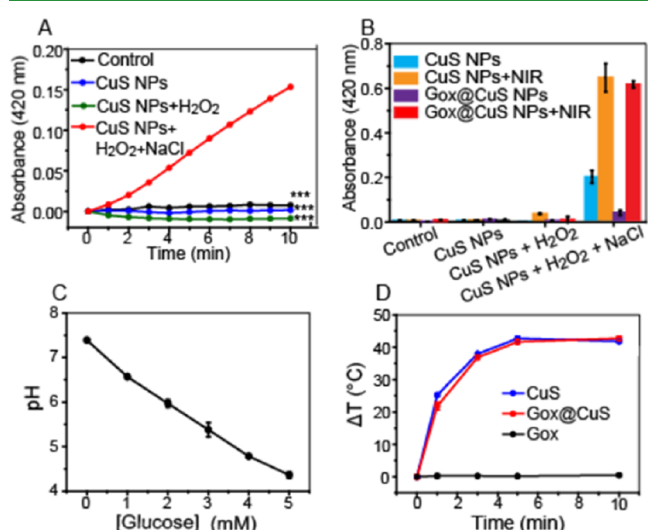


Figure 2. Catalytic activity of Gox@CuS nanoparticles (NPs). ABTS oxidation catalyzed by CuS NPs (10 $\mu\text{g}/\text{mL}$) (A) in the presence and absence of NaCl and (B) with or without NIR irradiation ($\lambda = 80$ nm and 1.5 W/cm^2). (C) Decrease in pH over 2 h as a function of glucose concentration. (D) Temperature change of the CuS NP solutions under NIR irradiation for 10 min. Error bars indicate standard deviation ($n = 3$).

Liu et al.,⁴³ ROS produced on the surface of CuS showed negligible activity toward the negatively charged ABTS compared to other substrates; however, the presence of Cl⁻ in this study demonstrated the accelerated oxidation of this probe by ROS under mildly acidic conditions provided by the glucose oxidation reaction catalyzed by Gox, as described in eq 1 (Figure S9). Importantly, we observed that this catalytic activity was primarily from the reactions facilitated by the NP surface and not from the acid-led degradation of H₂O₂, surface adsorption of ABTS, or leached Cu²⁺ (Figure S10).⁴⁴ The Cl⁻-accelerated Fenton reaction could be further enhanced via NIR irradiation, owing to the combination of local heating and electron–hole pairs generated by excitation of the CuS plasmon (Figure 2B). Although conjugation with Gox did inhibit the Fenton reaction significantly by blocking reactive sites on the NP surface, NIR irradiation was able to restore this activity (Figure 2B).

The catalytic activity of the surface-adsorbed Gox was confirmed by the reduction of pH resulting from gluconic acid generation (Figure 2C). In the presence of typical blood-glucose concentrations, the Gox@CuS NPs were able to reduce the pH of the buffered sample from physiological to mildly acidic conditions sufficient to activate the NP's Fenton-like activity. Meanwhile, H₂O₂ production also increased in a glucose dose-dependent manner (Figure S11). The H₂O₂ produced by Gox was catalytically decomposed by CuS NPs or Cu²⁺ within 1 h through Fenton-like chemistry (Figure S12), generating ROS, including superoxide radical anions (O₂^{•-}), •OH, and ¹O₂, which could induce oxidative damage to local biological structures. When considering the high levels of endogenous glucose and Cl⁻ in the interstitial fluid of solid tumors (~100–110 mM⁴⁵) as well as select organelles (e.g., ~118 mM in human lysosomes⁴⁶), Gox@CuS shows promise as a powerful nanocascade system. The ultimate products of H₂O₂ degradation catalyzed by the CuS NPs are H₂O and O₂, the latter of which is recycled back into glucose oxidation by Gox and the reformation of H₂O₂ (Scheme 1). Cancerous cells featuring normal or elevated levels of antioxidant enzymes, such as catalase and superoxide dismutase, are also expected to partially contribute to H₂O₂ production, degradation, and O₂ recycling through these enzymes.⁴⁷ In addition to the catalytic activity of the NPs, the temperatures of CuS and Gox@CuS NP solution increased ~40 °C within 5 min during NIR irradiation (Figure 2D), indicating a strong photothermal effect. The temperature increase not only kills cells directly but also enhances the Fenton reaction as previously mentioned (Figure 2B), contributing to the multimodal cancer therapy.

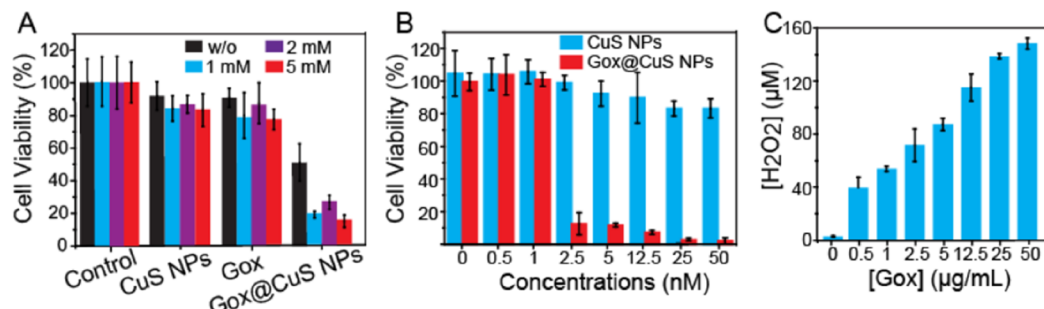


Figure 3. Toxicity of Gox@CuS nanoparticles (NPs) with different (A) glucose and (B) Gox@CuS NP concentrations toward B16F10 melanoma cells. (C) H₂O₂ produced by different Gox concentrations in the cell medium. Error bars indicate standard deviation ($n = 3$).

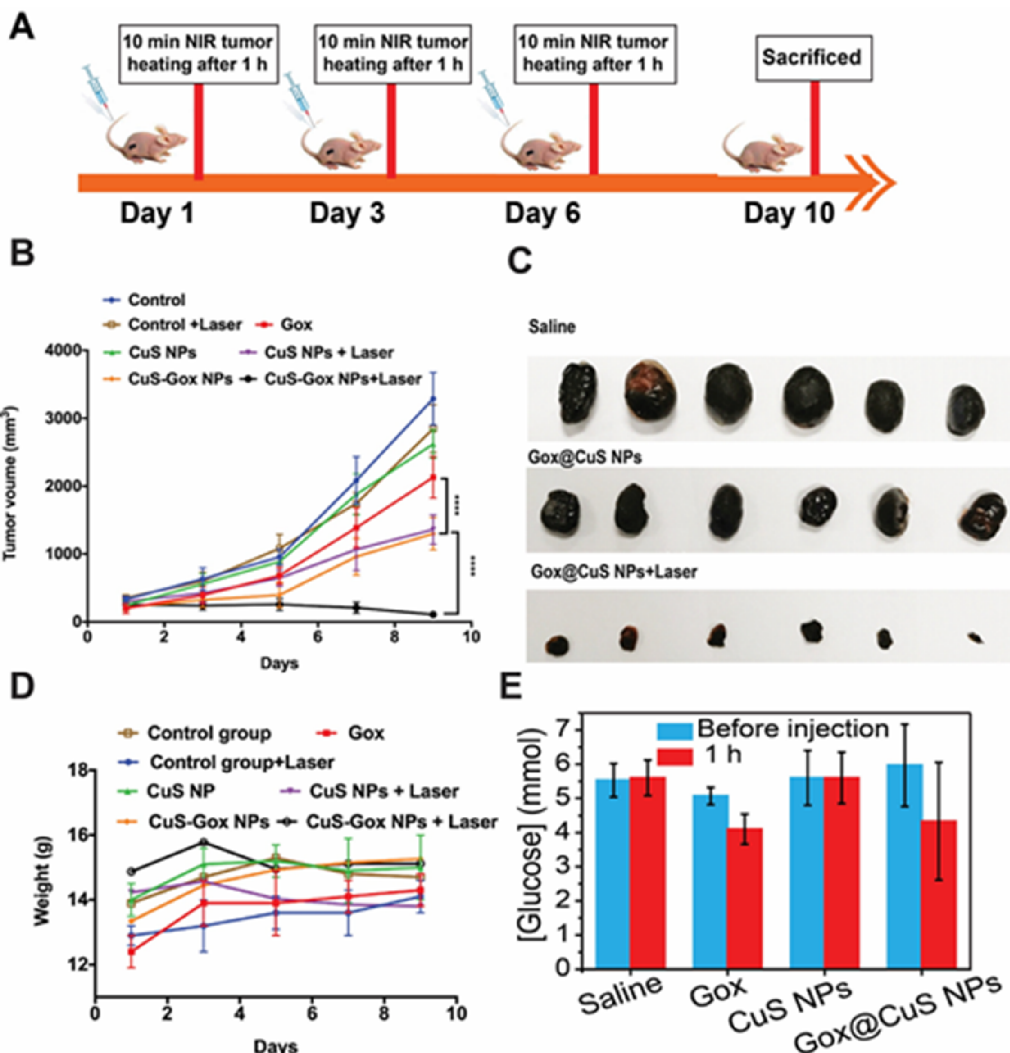


Figure 4. In vivo mouse model for efficacy evaluation of the Gox@CuS nanocomposite. (A) Schematic representation of in vivo antitumor experiments. (B) Tumor volume during the treatment. (C) Extracted tumor images after 9 days of treatment from sacrificed mice. (D) Mouse body weight during treatment. (E) Observed changes in the blood glucose level 1 h after treatment. Error bars indicate standard deviation ($n = 6$).

The synergistic therapeutic effects of Gox@CuS NPs were first demonstrated in two human cancer cell lines, i.e., melanoma B16F10 (Figure 3) and triple-negative breast cancer MDA-MB-231 (Figure S13) cell lines. The cells were treated with Gox, CuS NPs, or Gox@CuS nanocomposites in the presence of various glucose concentrations (0–5 mM). Only the Gox@CuS nanocomposite exhibited high cytotoxicity, which increased with higher glucose or nanocomposite concentrations (Figure 3). The anticancer effect of the nanocomposite was quite strong, with 2.5 nM (~0.19 $\mu\text{g}/\text{mL}$) Gox@CuS NPs capable of eliminating ~90% of the B16F10 cells during the short treatment period (Figure 3B). The composite also showed toxicity to cancerous cells when no exogenous glucose was added, where we presume that the toxicity was from the depletion of endogenous glucose and oxidative stress generated in the chain reaction that we would expect *in vivo*.

The Gox@CuS composite was significantly more effective than either CuS or Gox alone, with a calculated combination index of ~0.19 using the Chou–Talalay method, indicating the strong synergy of the chain reaction mechanism.^{48,49} H_2O_2 production in B16F10 cell medium was dependent on the Gox

concentration (Figure 3C). The IC_{50} values for B16F10 and MDA-MB-231 cells were calculated to be ~0.14 and 0.38 $\mu\text{g}/\text{mL}$, respectively. We then tested the activity enhancement of a brief NIR irradiation (5 s) with Gox@CuS treatment using confocal microscopy (Figure S14), which showed fewer viable cells after treatment than those treated with Gox, CuS, or Gox@CuS NPs alone. More ROS were generated inside cells treated with Gox@CuS NPs (with or without NIR irradiation), which was visible as bright green fluorescence and could be attributed to Cl-accelerated Fenton reactions. The uptake and photothermal performance of the CuS NPs by PC-3 prostate cancer cells were also evaluated. Following a 24 h incubation period with 30 $\mu\text{g}/\text{mL}$ CuS, ~17.7% (~5.3 $\mu\text{g}/\text{mL}$) was found to have been internalized or degraded by the cells using the CA-Fenton reaction in the media for quantification, whose standard curve is shown in Figure S5B. Following NIR irradiation (808 nm) at a power setting of 1 W/cm^2 for 5 min, cell viability was reduced from $61.7 \pm 7.26\%$ to $26.2 \pm 3.36\%$ (Figure S15). In comparison, NIR treatment alone showed no reduction in viability.

Because B16F10 cells showed a higher susceptibility toward the Gox@CuS treatment than MDA-MB-231 cells, we next

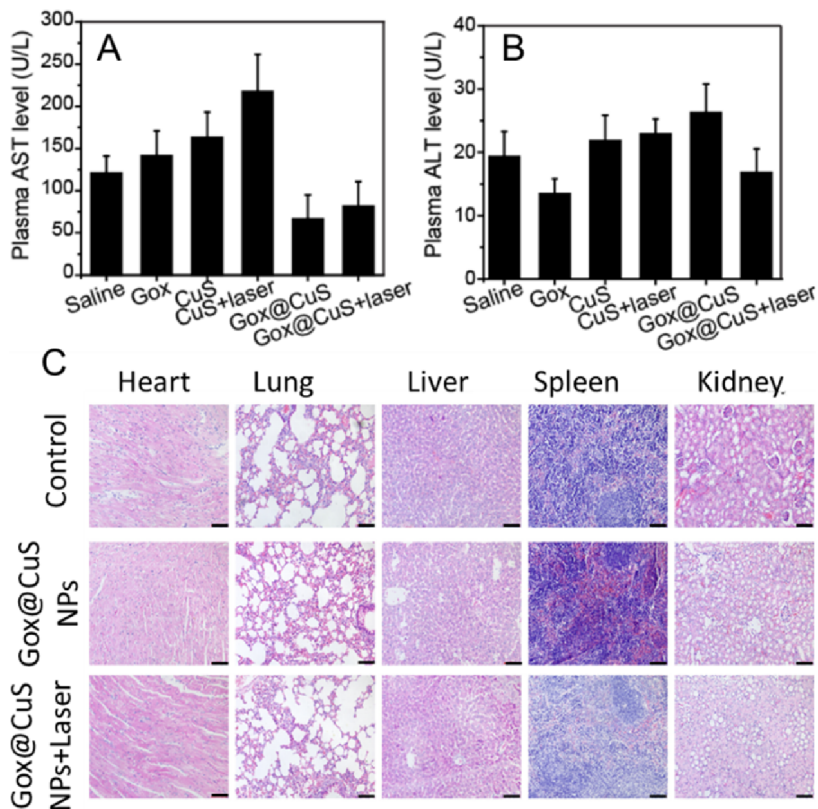


Figure 5. (A) AST and (B) ALT concentrations of healthy nude mice after 10 days of treatment to evaluate the liver function. (C) H&E staining of different organs of B16F10 tumor-bearing mice after 10 days of treatment. Scale bar = 100 μ m. Error bars indicate standard deviation ($n = 6$).

tested the therapeutic efficacy of the Gox@CuS nanocomposite using a mouse model of the melanoma B16F10 cells (Figure 4A). Tumor-bearing mice were randomly placed into seven groups (six mice per group) and treated with the following strategies: saline (negative control), saline + NIR irradiation, Gox, CuS NPs, CuS NPs + NIR irradiation, Gox@CuS, and Gox@CuS + NIR irradiation. Saline and the three individual therapeutic solutions (CuS and Gox@CuS NPs, 200 nM, 100 μ L, Gox = 2.2 mg/kg of body weight) were intravenously (IV) introduced into the mice. NIR irradiation (10 min, 5 W/cm²) was applied to the tumor area of the mice 1 h after injection. The change in body temperature was recorded with a forward-looking infrared camera. Although the camera measured the mouse skin temperature, their body temperature should exceed their skin temperature, and the images showed the accumulation of CuS and Gox@CuS NPs in the melanoma, which significantly increased the local tissue temperature under NIR irradiation (Figure S16). This low-temperature photothermal effect improved the suppression of tumor growth significantly (Figure 4B), attributable to both the locally produced heat and the NIR-enhanced catalytic activity of the CuS NPs and Gox@CuS nanocomposites (Figures 2B,D). In contrast, without NIR irradiation, CuS NPs did not inhibit tumor growth. When combined with NIR irradiation, the Gox@CuS nanocomposite showed the highest efficacy compared with the other groups, further demonstrating the synergistic effect of ST, Cl-accelerated Fenton-based CDT, and dual PDT-PTT for melanoma treatment (Figures 4B,C and S17).

No signs of acute systemic toxicity were observed as a result of treatment with Gox@CuS during the 10-day treatment period. First, no significant loss of body weight was observed

(Figure 4D). Second, the nanocomposite did not induce a noticeable or persistent drop of peripheral blood glucose after 1 h of IV injection (Figure 4E). Third, the blood aspartate aminotransferase (AST) and alanine aminotransferase (ALT) levels, indicators of the liver function, were not elevated (Figures 5A,B), indicating no harmful effect on the liver. Finally, potential pathological damage to the major organs, i.e., the heart, lungs, liver, spleen, and kidneys, by Gox@CuS + NIR treatment was evaluated using the histological images of the dissected organs. Compared to the saline-treated control group, no significant tissue damage was observed (Figure 5C), which further substantiated the biosafety of Gox@CuS NPs during treatment. After 10 days of treatment using Gox@CuS NPs + NIR, all tumor-bearing mice were cured (Figure S18) with only residual scar tissue remaining, while all other treatment groups retained some level of tumor growth. Overall, the results suggest the effectiveness and biosafety of the Gox@CuS nanocatalyst for tumor treatment.

3. CONCLUSIONS

Altogether, by integrating ST, Cl-accelerated CDT/PDT, and PTT using the Gox@CuS nanocomposite, a very simple, highly effective, and nontoxic nanomedicine formulation was demonstrated for synergistic combinatory cancer therapy. These unique attributes, especially the cost effectiveness and scalable fabrication, make the nanoformulation very promising for industrial manufacturing and clinical applications.

4. MATERIALS AND METHODS

4.1. Materials. Copper chloride dihydrate ($\text{CuCl}_2 \cdot 2\text{H}_2\text{O}$) was purchased from Shanghai Medin Co., Ltd. (Shanghai, China). Sodium citrate and glucose oxidase (Gox, Lot no. L470S90) were purchased

from J&K Chemical Co., Ltd. (Beijing, China). Sodium sulfide nonahydrate ($\text{Na}_2\text{S}\cdot 9\text{H}_2\text{O}$), 2,2'-azino-bis(3-ethylbenzothiazoline-6-sulfonate) (ABTS), fluorometric H_2O_2 assay kit (catalog no. 187 037), and HEPES buffer were purchased from Sigma-Aldrich Co., Ltd. (Shanghai, China). Cell growth media (DMEM and RPMI-1640) were purchased from Thermo Fisher Scientific (Waltham, MA, USA). CCK-8 and (3-(4,5-dimethylthiazol-2-yl)-2,5-diphenyltetrazolium bromide (MTT) were purchased from Beyotime Co., Ltd. (Jiangsu, China). Liver toxicity assay kits (ALT and AST assay kits) were obtained from Elabscience Biotechnology Co. Ltd. (Wuhan, China). Fetal bovine serum (FBS) was obtained from Invitrogen Life Technologies (Carlsbad, CA, USA). Human breast cancer MD-MB-231 and melanoma cell line B16F10 were obtained from China Infrastructure of Cell Line Resource (Beijing, China). CellROX green reagent was purchased from Life Technologies Inc. (Grand Island, NY, USA). Hoechst 33258 was obtained from Thermo Scientific (Waltham, MA, USA).

4.2. Gox@CuS NP Fabrication. Citrate-capped CuS NPs were synthesized using a previously reported method with slight modifications.³⁰ Briefly, $\text{CuCl}_2\cdot 2\text{H}_2\text{O}$ (10.77 mg) and trisodium citrate (10 mg) were dissolved in 30 mL of nanopure water (prepared by a Milli-Q water purification system, Merck). After 15 min of stirring, 50 μL of aqueous $\text{Na}_2\text{S}\cdot 9\text{H}_2\text{O}$ (743.92 mg/mL) was rapidly added to the solution under vigorous stirring. The solution was transferred to a water bath (90 °C) and stirred for an additional 30 min until the solution turned dark green, indicating the formation of CuS NPs. The synthesized NPs were purified from the crude mixture via overnight dialysis against nanopure water. The amount of synthesized CuS was determined by measuring the free Cu ions remaining in the crude mixture using the colorimetric method previously developed by our group.³⁵ Briefly, to separate the free Cu ions from the highly dispersible NPs, an equal volume of ethanol containing 100 mM NaCl was added to the crude NP mixture and centrifuged at 10 000 rpm for 10 min. The clear supernatant was carefully removed, diluted, and then added to a series of CuCl_2 standard solutions (final concentration 0–200 nM) for analysis. Afterward, 20 μL of each standard solution was added to a mixture containing the substrate 3,3',5,5'-tetramethylbenzidine (TMB, 750 mM), NaCl (100 mM), and MES buffer (2 mM, pH 5.5). As a result of TMB, DMSO composed 10% of the final reaction volume. To this, 50 μL of 3% H_2O_2 was then added to bring the final volume to 200 μL . Immediately after adding H_2O_2 , the oxidation of TMB was monitored at 650 nm using a Tecan Infinite M1000 PRO microplate reader (Mannedorf, Switzerland) and the concentration of Cu in the sample was calculated ($n = 3$).

Gox (10 mg) was conjugated onto the CuS NPs by adding it to 30 mL of the prepared CuS NPs and shaking for 10 min. The conjugate material was then separated from the free NPs and enzymes by size-exclusion chromatography using Sephadex G-50 pre-equilibrated with Milli-Q water and 0.1× PBS (pH 7.4). After separation, the nanocomposite was freeze-dried and stored in a freezer (−20 °C) for future use. To determine the loading capacity of Gox on the CuS NPs, the Bradford assay was used to calculate the unconjugated protein remaining following conjugate synthesis and separation ($n = 3$).

4.3. Characterization of CuS NPs. **4.3.1. Particle Size and Zeta Potential Measurement.** The particle size and surface charge of the freshly synthesized CuS NPs and Gox@CuS NPs were measured using a Malvern Zetasizer, Nano series (Nano ZS90) in triplicate.

4.3.2. Optical Characterization. The UV-vis and IR spectra of CuS NPs and Gox@CuS NPs were measured using a UV-vis–NIR spectrophotometer (Shimadzu, UV-3600 plus 220/230 VC) and a Thermo Scientific Nicolet FT-IR spectrophotometer in the region of 4000–400 cm^{-1} , respectively. The data were processed using Origin Pro 8 software.

4.3.3. Gox@CuS NP Structure and Composition. The morphological characterization of the as-synthesized NPs was performed using TEM (JEM-1400 TEM, 40–120 kV). To check the composition of Gox@CuS NPs, EDX analysis was also performed.

4.4. pH Effect of Gox@CuS NPs. To measure the ability of the Gox@CuS conjugates to reduce the pH of the local environment ($n = 3$), 500 μL of the Gox@CuS conjugates was added to 4.5 mL of 0.1× PBS (pH 7.44) containing various concentrations of glucose (0–5 mM). The solutions were incubated for 2 h at ambient temperature with gentle shaking, and the pH was monitored using a pH meter.

4.5. In Vitro Photothermal Activity of CuS NPs. To determine the photothermal activity of the NPs, 200 μL of Gox, CuS NPs, or Gox@CuS NPs was added to a 96-well plate and irradiated with an 808 nm diode laser (1.5 W/cm²) for up to 10 min. The temperature of the various solutions was measured using a digital thermometer. For thermal imaging, solutions of PBS, CuS NPs, and Gox@CuS NPs were taken in a microtube and subjected to NIR irradiation (980 nm, 5 W/cm²) for 5 min. Then, the temperature change of the NP solutions was recorded using a forward-looking IR camera (class 2 laser product, FDA approved). The thermal images were further processed using Image J software.

For analysis of PC-3 cells ($n = 3$), 5000 cells were seeded per well in a 96-well plate and allowed to attach for 24 h before being introduced to CuS NPs (30 $\mu\text{g}/\text{mL}$). After a further 24 h, the cells were exposed to an 808 nm diode laser (1 W/cm²) for 5 min. The cells were then washed with PBS and allowed to grow for another 24 h, after which the viability was assessed via the MTT assay with cells not exposed to CuS NPs serving as a comparison.

4.6. Fenton-like Catalytic Activity of CuS NPs. To evaluate the catalytic properties of CuS NPs under various conditions, the kinetics of the oxidation of the chromogenic substrate molecule ABTS (2,2'-azino-bis(3-ethylbenzothiazoline-6-sulfonate)) was recorded with light absorbance at $\lambda_{3bb} = 420$ nm using a Tecan Infinite M1000 PRO microplate reader (Mannedorf, Switzerland) for the oxidized ABTS. The kinetics of this reaction were investigated at different pH values and H_2O_2 and glucose concentrations, in the presence or absence of NaCl, with or without NIR irradiation.

Generally, all experiments ($n = 3$) were performed in 96-well microplates with a final reaction volume of 200 μL . The oxidation of 250 μM ABTS was monitored at 420 nm in the presence or absence of one or more of the following: CuS NPs or Gox@CuS NPs (10 $\mu\text{g}/\text{mL}$), NaCl (100 mM), and H_2O_2 (200 mM). The pH was adjusted between 3.6 and 5.6 using differently buffered 0.1 M acetate buffers. Reactions at pH 6–8 were conducted using 0.1× phosphate buffer. NIR excitation was achieved by exposing the sample wells to a diode laser (808 nm, 1.5 W/cm²) continuously for 3 min. An appropriate amount of water was added following laser excitation to account for evaporation from the photothermal effect.

To study whether the Fenton reactivity was from the Gox@CuS nanocomposite or leached Cu^{2+} , the separated Gox@CuS nanocomposite was added to acetate buffer (10 mM, pH 4.0) containing 300 mM NaCl and incubated for 30 min at ambient temperature before centrifuging the solutions to precipitate the Gox@CuS NPs and collect the supernatant. The precipitated Gox@CuS NPs were redispersed in the same volume of acetate buffer. Afterward, the same volumes of Gox@CuS NPs and supernatant were tested for their catalytic reactivity in the Fenton reaction with or without 5 min NIR irradiation, where the final concentrations of ABTS, H_2O_2 , and NaCl were 250 μM , 200 mM, and 300 mM, respectively.

A H_2O_2 assay was performed to determine the H_2O_2 production by Gox at different glucose concentrations. Briefly, 30 μL of different glucose concentrations and 20 μL of 10 $\mu\text{g}/\text{mL}$ Gox or an equivalent amount of Gox@CuS were added to 50 μL of H_2O_2 assay buffer (Sigma-Aldrich, USA), and the fluorescence of the samples was measured at $\lambda_{\text{em}} = 590$ nm ($\lambda_{\text{ex}} = 540$ nm). The catalytic properties of the CuS NPs were also measured for different time periods. All of the samples were measured in triplicate.

4.7. Cell-Killing Activity of CuS NPs. MDA-MB-231 and PC-3 cells were cultured in the complete RPMI-1640 medium, containing 2000 mg/L glucose, 10% FBS, and 100 U/mL penicillin and streptomycin. B16F10 cells were cultured in high-glucose (4500 mg/L) DMEM supplemented with 10% FBS and 100 U/mL penicillin and streptomycin. The cells were incubated at 37 °C in a humidified 5% CO₂ atmosphere. The media were changed every 2 days during

incubation. Cells for experiments were taken from an exponentially growing phase and harvested from plates with trypsin–EDTA. The cells were counted using a hemocytometer.

To check the *in vitro* cytotoxicity of Gox@CuS NPs ($n = 3$), B16F10 and MDA-MB-231 cells were seeded into 96-well plates (5000 cells/well) and incubated for 24 h in cell media for attachment. Subsequently, the media were replaced and supplemented with 10 μ L of Gox@CuS NPs (0.25, 0.5, 1, 2.5, 5, 10, 25, and 50 nM) prepared in HEPES buffer. After 12 h of incubation, the MTT reagent was added to each well and incubated for another 4 h. Afterward, the cells were gently washed with PBS three times and replaced with 200 μ L of DMSO to dissolve the formazan crystals, whose absorbance was measured at 590 nm and 650 nm using a microplate reader (SpectraMax M5e, Molecular Devices, San Jose, CA, USA). Similarly, we analyzed the cytotoxicity at different glucose concentrations.

4.8. H_2O_2 Production by Gox. The H_2O_2 concentration produced in cell medium by Gox was quantified with a fluorometric H_2O_2 assay kit. B16F10 cells were cultured in DMEM (containing 4.5 g/L glucose) and seeded into 96-well plates (5000 cells/well; $n = 3$). After 24 h, Gox solutions of different concentrations were added to each well and incubated for a further 12 h. Then, 20 μ L of the medium was added to another 96-well plate containing 30 μ L of nanopure water. To quantify H_2O_2 , 50 μ L of the H_2O_2 detection reagent was added and incubated in the dark for 30 min. The fluorescence intensity of the samples was finally measured at 590 nm (λ_{ex} 540 nm) using a microplate reader. The concentration was quantified against H_2O_2 standard solutions.

4.9. Intracellular ROS Levels. The detection of intracellular ROS analysis was performed with B16F10 cells. After the B16F10 cells were incubated with Gox, CuS with or without the laser (30 s of irradiation without increasing the medium temperature), and Gox@CuS with or without the laser, they were treated with CellROX Green Reagent according to the manufacturer's instructions. Then, the treated cells were fixed in 4% (w/v) paraformaldehyde for 10 min and stained with Hoechst 33258 staining solution (5 μ g/mL). After rinsing with PBS, images were taken using a confocal laser scanning microscope (Nikon, Japan) with the excitation channels at 405 and 488 nm for the quantitative determination of ROS levels. The fluorescence intensity was analyzed using ImageJ software.

4.10. In Vitro Uptake. Quantification of the amount of CuS NPs internalized by cells was performed using PC-3 cells. To detect the NPs, a variation of our method for detecting Cu^{2+} ions was used. Briefly, after incubating the CuS NPs for 24 h in RPMI-1640 media (10% FBS) with or without cells (5000 cells/well in triplicate), the media were carefully removed and analyzed for the oxidation of TMB at 652 nm. NPs incubated without cells were serially diluted to form a standard curve, and the amount of CuS NPs not internalized or degraded by cells (i.e., remaining in the media) was calculated based on the relative rate of oxidation.

4.11. In Vivo Evaluation of the Synergistic Cancer Therapy. All of the animal studies were performed in the Laboratory Animal Center, Cancer Hospital, Chinese Academy of Medical Sciences, Shenzhen Center. The experimental procedures were based on the guidelines on animal care and use of Principles of Laboratory Animal Care (NIH publication no. 86-23, revised 1985) and approved by the Institutional Animal Care Committee at Cancer Hospital, Chinese Academy of Medical Sciences, Shenzhen Center (no. NCC2019A006).

Male BALB/c-nu/nu mice (11–13 g, 21–28 days) were supplied by the Southern Medical School Laboratory Animal Center (no. 44002100020556). When their body weight reached 15–18 g, 0.1 mL of B16F10 cells (10^6 cells/mL) was injected into the back of each mouse to establish the subcutaneous tumor xenografts. The tumors were allowed to grow to a size of 80–100 mm³ before the start of the experiment. For therapeutic evaluation, all of the mice were randomly assigned into seven groups ($n = 6$): (1) saline, (2) saline with NIR irradiation, (3) Gox, (4) CuS NPs, (5) CuS-NPs with NIR laser irradiation, (6) Gox@CuS NPs, and (7) Gox@CuS NPs with NIR laser irradiation. The mice were injected with 100 μ L of saline solution from the tail vein.

The Gox@CuS NPs along with control (saline solution) were injected into the mice IV via the tail vein. The body weights and tumor volumes were measured on alternate days to evaluate the therapeutic efficacy. The Gox (2.2 mg/kg body weight) and Gox@CuS NPs (200 nM; 100 μ L; dosage, 2 μ g/kg body weight) were injected on alternate days. After 1 h of drug administration, NIR laser irradiation was applied on the tumor site for 10 min at a power setting of 5 W/cm². After 10 days, the mice were sacrificed, and the tumors were separated from the skin. Their blood was collected for liver toxicity and blood glucose level determination. The blood glucose level of the mice was measured with a glucometer before and after administration of the therapeutics.

4.12. Liver Toxicity Assay. The day after the last treatment, the blood of each group's mice was collected directly from the eyes 24 h postinjection. The blood samples were stored at 4 °C overnight and centrifuged at 3000 rpm for 20 min to separate the plasma. The plasma levels of AST and ALT in mice were assayed according to the protocols recommended by the manufacturer. The absorbance was measured with a plate reader at 510 nm.

4.13. Histological Analysis. Histological analysis of different organs was performed using a microscope for which tissue samples of different organs were collected and fixed with paraformaldehyde (3%). The biopsies were embedded into paraffin blocks and then sliced into sections (~4 μ m). These sections were stained with H&E for histological examination. The stained sections were observed under a bright light field with a microscope (Leica DM6b, Germany), and the images were processed using Leica LAS X software.

4.14. Statistical Analysis. Data were expressed as mean values with standard deviation. One-way ANOVA was used to compare two or multiple groups, and $p < 0.05$ was considered significant.

ASSOCIATED CONTENT

Supporting Information

The Supporting Information is available free of charge at <https://pubs.acs.org/doi/10.1021/acsami.1c12235>.

TEM images, zeta potential, DLS measurements, FTIR spectra, standard curves, *in vitro* and *in vivo* thermal camera images, Fenton catalytic activity, cell viability of PC-3 prostate cancer cells after treatment, EDX analysis, additional oxidation reactions under varying conditions, leached Cu^{2+} detection, *in vitro* H_2O_2 production, MDA-MB-231 cell viability, photothermal therapy of PC-3 cells, tumor and mice images following treatment, EDX analysis, and literature comparison ([PDF](#))

AUTHOR INFORMATION

Corresponding Authors

Runqing Jiang – Grand River Regional Cancer Centre, Kitchener, Ontario N2G 1G3, Canada;
Email: Runqing.jiang@grhosp.on.ca

Xu Zhang – Department of Chemistry, Cape Breton University, Sydney, Nova Scotia B1P 6L2, Canada;
orcid.org/0000-0002-8098-0410; Email: Xu_zhang@cbu.ca

Authors

Parbeen Singh – Postdoctoral Innovation Practice Base, Shenzhen Key Laboratory of Fermentation, Purification and Analysis and Department of Biological Applied Engineering, Shenzhen Key Laboratory of Fermentation, Purification and Analysis, Shenzhen Polytechnic, Shenzhen 518055, China

Brian Youden – Department of Chemistry, Cape Breton University, Sydney, Nova Scotia B1P 6L2, Canada;
Department of Biology, University of Waterloo, Waterloo,

Ontario N2L 3G1, Canada;  orcid.org/0000-0003-2545-2866

Yikun Yang — National Cancer Center/National Clinical Research Center for Cancer/Cancer Hospital & Shenzhen Hospital, Chinese Academy of Medical Sciences and Peking Union Medical College, Shenzhen 518116, China

Yongli Chen — Postdoctoral Innovation Practice Base, Shenzhen Key Laboratory of Fermentation, Purification and Analysis and Department of Biological Applied Engineering, Shenzhen Key Laboratory of Fermentation, Purification and Analysis, Shenzhen Polytechnic, Shenzhen 518055, China

Andrew Carrier — Department of Chemistry, Cape Breton University, Sydney, Nova Scotia B1P 6L2, Canada

Shufen Cui — Department of Biological Applied Engineering, Shenzhen Key Laboratory of Fermentation, Purification and Analysis, Shenzhen Polytechnic, Shenzhen 518055, China

Ken Oakes — Department of Biology, Cape Breton University, Sydney, Nova Scotia B1P 6L2, Canada

Mark Servos — Department of Biology, University of Waterloo, Waterloo, Ontario N2L 3G1, Canada

Complete contact information is available at:

<https://pubs.acs.org/10.1021/acsami.1c12235>

Author Contributions

#P.S. and B.Y. contributed equally to this work. P. S. and B. Y.: Methodology, validation, analysis, investigation, data curation, visualization, writing – original draft preparation, and writing – reviewing and editing. Y. Y.: Methodology, investigation. Y. C.: Conceptualization, methodology, analysis, investigation, data curation, visualization, writing – original draft preparation, and project administration. A. C.: Analysis, methodology, and writing – reviewing and editing. S. C.: Supervision, resources, project administration, and funding acquisition. K. O.: Supervision, writing – reviewing and editing, and funding acquisition. M. S. and R. J.: Supervision, resources, writing – reviewing and editing, and funding acquisition. X. Z.: Conceptualization, methodology, formal analysis, writing – original draft preparation, writing – reviewing and editing, supervision, project administration, and funding acquisition.

Notes

The authors declare no competing financial interest.

ACKNOWLEDGMENTS

This work was supported by the China Postdoctoral Science Foundation (nos. 2019M653139 and 2019M653979), Guangdong Province Higher Vocational College and Schools Pearl River Scholar Funded Scheme (2017), the Canada Research Chairs Program, New Frontiers in Research Fund—Exploration (no. NFRFE-2018-01005), the Project of Scientific and Technological Foundation of Shenzhen, China (no. GJHZ20180928161212140), Cape Breton University RISE program, NSERC Discovery Grants Program, Canada's Telus Ride for Dad (RFD) and The Prostate Cancer Fight Foundation (PCFF), and the Post-doctoral Foundation Project of Shenzhen Polytechnic (nos. 6019330001K, 6019330006K, and 6019330007K).

REFERENCES

- (1) Dizon, D. S.; Hensley, M. L.; Poynor, E. A.; Sabbatini, P.; Aghajanian, C.; Hummer, A.; Venkatraman, E.; Spriggs, D. R. Retrospective Analysis of Carboplatin and Paclitaxel as Initial Second-Line Therapy for Recurrent Epithelial Ovarian Carcinoma: Application toward a Dynamic Disease State Model of Ovarian Cancer. *J. Clin. Oncol.* **2002**, *20*, 1238–1247.
- (2) Pienta, K. J.; Partin, A. W.; Coffey, D. S. Cancer as a Disease of DNA Organization and Dynamic Cell Structure. *Cancer Res.* **1989**, *49*, 2525–2532.
- (3) Fan, W.; Yung, B.; Huang, P.; Chen, X. Nanotechnology for Multimodal Synergistic Cancer Therapy. *Chem. Rev.* **2017**, *117*, 13566–13638.
- (4) Wang, M.; Wang, D.; Chen, Q.; Li, C.; Li, Z.; Lin, J. Recent Advances in Glucose-Oxidase-Based Nanocomposites for Tumor Therapy. *Small* **2019**, *15*, No. 1903895.
- (5) Fu, L.-H.; Qi, C.; Lin, J.; Huang, P. Catalytic Chemistry of Glucose Oxidase in Cancer Diagnosis and Treatment. *Chem. Soc. Rev.* **2018**, *47*, 6454–6472.
- (6) Gao, P.; Shi, M.; Wei, R.; Pan, W.; Liu, X.; Li, N.; Tang, B. A Biomimetic MOF Nanoreactor Enables Synergistic Suppression of Intracellular Defense Systems for Augmented Tumor Ablation. *Chem. Commun.* **2020**, *S6*, 924–927.
- (7) Yu, Z.; Zhou, P.; Pan, W.; Li, N.; Tang, B. A Biomimetic Nanoreactor for Synergistic Chemiexcited Photodynamic Therapy and Starvation Therapy Against Tumor Metastasis. *Nat. Commun.* **2018**, *9*, No. 5044.
- (8) Hanahan, D.; Weinberg, R. A. Hallmarks of Cancer: The Next Generation. *Cell* **2011**, *144*, 646–674.
- (9) Bubici, C.; Papa, S. Editorial: The Warburg Effect Regulation Under Siege: The Intertwined Pathways in Health and Disease. *Front. Cell Dev. Biol.* **2019**, *7*, No. 80.
- (10) Denko, N. C. Hypoxia, HIF1 and Glucose Metabolism in the Solid Tumour. *Nat. Rev. Cancer* **2008**, *8*, 705–713.
- (11) Vander Heiden, M. G.; Cantley, L. C.; Thompson, C. B. Understanding the Warburg Effect: The Metabolic Requirements of Cell Proliferation. *Science* **2009**, *324*, 1029–1033.
- (12) Carrier, A.; Nganou, C.; Oakley, D.; Chen, Y.; Oakes, K.; MacQuarrie, S.; Zhang, X. Selective Generation of Singlet Oxygen in Chloride Accelerated Copper Fenton Chemistry. *Catalysis* **2018**, DOI: [10.26434/chemrxiv.7364225.v1](https://doi.org/10.26434/chemrxiv.7364225.v1) (accessed Aug 14, 2021)
- (13) Carrier, A.; Hamid, S.; Oakley, D.; Oakes, K.; Zhang, X. Singlet Oxygen Generation in Classical Fenton Chemistry. *Catalysis* **2019**, DOI: [10.26434/chemrxiv.7730654.v1](https://doi.org/10.26434/chemrxiv.7730654.v1) (accessed Aug 14, 2021).
- (14) Huo, M.; Wang, L.; Chen, Y.; Shi, J. Tumor-Selective Catalytic Nanomedicine by Nanocatalyst Delivery. *Nat. Commun.* **2017**, *8*, No. 357.
- (15) Zhang, C.; Zhang, L.; Wu, W.; Gao, F.; Li, R.-Q.; Song, W.; Zhuang, Z.-N.; Liu, C.-J.; Zhang, X.-Z. Artificial Super Neutrophils for Inflammation Targeting and HClO Generation against Tumors and Infections. *Adv. Mater.* **2019**, *31*, No. e1901179.
- (16) Fan, W.; Lu, N.; Huang, P.; Liu, Y.; Yang, Z.; Wang, S.; Yu, G.; Liu, Y.; Hu, J.; He, Q.; Qu, J.; Wang, T.; Chen, X. Glucose-Responsive Sequential Generation of Hydrogen Peroxide and Nitric Oxide for Synergistic Cancer Starving-Like/Gas Therapy. *Angew. Chem., Int. Ed.* **2017**, *S6*, 1229–1233.
- (17) Wang, C.; Yang, J.; Dong, C.; Shi, S. Glucose Oxidase-Related Cancer Therapies. *Adv. Ther.* **2020**, *3*, No. 2000110.
- (18) Li, S.-Y.; Cheng, H.; Xie, B.-R.; Qiu, W.-X.; Zeng, J.-Y.; Li, C.-X.; Wan, S.-S.; Zhang, L.; Liu, W.-L.; Zhang, X.-Z. Cancer Cell Membrane Camouflaged Cascade Bioreactor for Cancer Targeted Starvation and Photodynamic Therapy. *ACS Nano* **2017**, *11*, 7006–7018.
- (19) Bonifert, G.; Folkes, L.; Gmeiner, C.; Dachs, G.; Spadiut, O. Recombinant Horseradish Peroxidase Variants for Targeted Cancer Treatment. *Cancer Med.* **2016**, *5*, 1194–1203.
- (20) Ranji-Burachaloo, H.; Gurr, P. A.; Dunstan, D. E.; Qiao, G. G. Cancer Treatment through Nanoparticle-Facilitated Fenton Reaction. *ACS Nano* **2018**, *12*, 11819–11837.
- (21) Tan, H.; Guo, S.; Dinh, N.-D.; Luo, R.; Jin, L.; Chen, C.-H. Heterogeneous Multi-Compartmental Hydrogel Particles as Synthetic Cells for Incompatible Tandem Reactions. *Nat. Commun.* **2017**, *8*, No. 663.

- (22) Xiang, H.; Feng, W.; Chen, Y. Single-Atom Catalysts in Catalytic Biomedicine. *Adv. Mater.* **2020**, *32*, No. 1905994.
- (23) Yang, B.; Ding, L.; Yao, H.; Chen, Y.; Shi, J. A Metal-Organic Framework (MOF) Fenton Nanoagent-Enabled Nanocatalytic Cancer Therapy in Synergy with Autophagy Inhibition. *Adv. Mater.* **2020**, *32*, No. 1907152.
- (24) Zhou, J.; Li, M.; Hou, Y.; Luo, Z.; Chen, Q.; Cao, H.; Huo, R.; Xue, C.; Sutrisno, L.; Hao, L.; Cao, Y.; Ran, H.; Lu, L.; Li, K.; Cai, K. Engineering of a Nanosized Biocatalyst for Combined Tumor Starvation and Low-Temperature Photothermal Therapy. *ACS Nano* **2018**, *12*, 2858–2872.
- (25) Fu, L.-H.; Hu, Y.-R.; Qi, C.; He, T.; Jiang, S.; Jiang, C.; He, J.; Qu, J.; Lin, J.; Huang, P. Biodegradable Manganese-Doped Calcium Phosphate Nanotheranostics for Traceable Cascade Reaction-Enhanced Anti-Tumor Therapy. *ACS Nano* **2019**, *13*, 13985–13994.
- (26) Zhang, Y.; Yang, Y.; Jiang, S.; Li, F.; Lin, J.; Wang, T.; Huang, P. Degradable Silver-Based Nanoplatform for Synergistic Cancer Starving-like/Metal Ion Therapy. *Mater. Horiz.* **2019**, *6*, 169–175.
- (27) Zhang, Y.; Wang, F.; Liu, C.; Wang, Z.; Kang, L.; Huang, Y.; Dong, K.; Ren, J.; Qu, X. Nanozyme Decorated Metal–Organic Frameworks for Enhanced Photodynamic Therapy. *ACS Nano* **2018**, *12*, 651–661.
- (28) Zhang, Y.-H.; Qiu, W.-X.; Zhang, M.; Zhang, L.; Zhang, X.-Z. MnO₂ Motor: A Prospective Cancer-Starving Therapy Promoter. *ACS Appl. Mater. Interfaces* **2018**, *10*, 15030–15039.
- (29) Feng, L.; Xie, R.; Wang, C.; Gai, S.; He, F.; Yang, D.; Yang, P.; Lin, J. Magnetic Targeting, Tumor Microenvironment-Responsive Intelligent Nanocatalysts for Enhanced Tumor Ablation. *ACS Nano* **2018**, *12*, 11000–11012.
- (30) Dong, L.; Li, K.; Wen, D.; Lu, Y.; Du, K.; Zhang, M.; Gao, X.; Feng, J.; Zhang, H. A Highly Active (102) Surface-Induced Rapid Degradation of a CuS Nanotheranostic Platform for in Situ T1-Weighted Magnetic Resonance Imaging-Guided Synergistic Therapy. *Nanoscale* **2019**, *11*, 12853–12857.
- (31) Li, Y.; Lu, W.; Huang, Q.; Li, C.; Chen, W. Copper Sulfide Nanoparticles for Photothermal Ablation of Tumor Cells. *Nanomedicine* **2010**, *5*, 1161–1171.
- (32) Wang, S.; Riedinger, A.; Li, H.; Fu, C.; Liu, H.; Li, L.; Liu, T.; Tan, L.; Barthel, M. J.; Pugliese, G.; De Donato, F.; Scotto D'Abbusco, M.; Meng, X.; Manna, L.; Meng, H.; Pellegrino, T. Plasmonic Copper Sulfide Nanocrystals Exhibiting Near-Infrared Photothermal and Photodynamic Therapeutic Effects. *ACS Nano* **2015**, *9*, 1788–1800.
- (33) Ku, G.; Zhou, M.; Song, S.; Huang, Q.; Hazle, J.; Li, C. Copper Sulfide Nanoparticles as a New Class of Photoacoustic Contrast Agent for Deep Tissue Imaging at 1064 nm. *ACS Nano* **2012**, *6*, 7489–7496.
- (34) Yi, X.; Chen, L.; Chen, J.; Maiti, D.; Chai, Z.; Liu, Z.; Yang, K. Biomimetic Copper Sulfide for Chemo-Radiotherapy: Enhanced Uptake and Reduced Efflux of Nanoparticles for Tumor Cells under Ionizing Radiation. *Adv. Funct. Mater.* **2018**, *28*, No. 1705161.
- (35) Shan, Z.; Lu, M.; Wang, L.; MacDonald, B.; MacInnis, J.; Mkandawire, M.; Zhang, X.; Oakes, K. D. Chloride Accelerated Fenton Chemistry for the Ultrasensitive and Selective Colorimetric Detection of Copper. *Chem. Commun.* **2016**, *52*, 2087–2090.
- (36) Wang, L.; Hou, J.; Liu, S.; Carrier, A. J.; Guo, T.; Liang, Q.; Oakley, D.; Zhang, X. CuO Nanoparticles as Haloperoxidase-Mimics: Chloride-Accelerated Heterogeneous Cu-Fenton Chemistry for H₂O₂ and Glucose Sensing. *Sens. Actuators, B* **2019**, *287*, 180–184.
- (37) Wang, L.; Miao, Y.; Lu, M.; Shan, Z.; Lu, S.; Hou, J.; Yang, Q.; Liang, X.; Zhou, T.; Curry, D.; Oakes, K.; Zhang, X. Chloride-Accelerated Cu-Fenton Chemistry for Biofilm Removal. *Chem. Commun.* **2017**, *53*, 5862–5865.
- (38) Li, Y.; Zhao, J.; Shang, E.; Xia, X.; Niu, J.; Crittenden, J. Effects of Chloride Ions on Dissolution, ROS Generation, and Toxicity of Silver Nanoparticles under UV Irradiation. *Environ. Sci. Technol.* **2018**, *52*, 4842–4849.
- (39) Choudhary, V. R.; Samanta, C. Role of Chloride or Bromide Anions and Protons for Promoting the Selective Oxidation of H₂ by O₂ to H₂O₂ over Supported Pd Catalysts in an Aqueous Medium. *J. Catal.* **2006**, *238*, 28–38.
- (40) Rainieri, M.; Winkler, E. L.; Torres, T. E.; Vasquez Mansilla, M.; Nadal, M. S.; Zysler, R. D.; Lima, E. Effects of Biological Buffer Solutions on the Peroxidase-like Catalytic Activity of Fe₃O₄ Nanoparticles. *Nanoscale* **2019**, *11*, 18393–18406.
- (41) Chen, L.; Hu, H.; Chen, Y.; Gao, J.; Li, G. Plasmonic Cu₂-S Nanoparticles: A Brief Introduction of Optical Properties and Applications. *Mater. Adv.* **2021**, *2*, 907–926.
- (42) Nichela, D. A.; Berkovic, A. M.; Costante, M. R.; Juliarena, M. P.; Garcia Einschlag, F. S. Nitrobenzene Degradation in Fenton-like Systems Using Cu(II) as Catalyst. Comparison between Cu(II)- and Fe(III)-Based Systems. *Chem. Eng. J.* **2013**, *228*, 1148–1157.
- (43) Liu, Y.; Jin, H.; Zou, W.; Guo, R. Protein-Mediated Sponge-like Copper Sulfide as an Ingenious and Efficient Peroxidase Mimic for Colorimetric Glucose Sensing. *RSC Adv.* **2020**, *10*, 28819–28826.
- (44) Guan, J.; Peng, J.; Jin, X. Synthesis of Copper Sulfide Nanorods as Peroxidase Mimics for the Colorimetric Detection of Hydrogen Peroxide. *Anal. Methods* **2015**, *7*, 5454–5461.
- (45) Gullino, P. M.; Clark, S. H.; Grantham, F. H. The Interstitial Fluid of Solid Tumors. *Cancer Res.* **1964**, *24*, 780–794.
- (46) Chakraborty, K.; Leung, K.; Krishnan, Y. High Luminal Chloride in the Lysosome is Critical for Lysosome Function. *Elife* **2017**, *6*, No. e28826.
- (47) Glorieux, C.; Zamocky, M.; Sandoval, J. M.; Verrax, J.; Calderon, P. B. Regulation of Catalase Expression in Healthy and Cancerous Cells. *Free Radicals Biol. Med.* **2015**, *87*, 84–97.
- (48) Fan, Z.; Jiang, B.; Zhu, Q.; Xiang, S.; Tu, L.; Yang, Y.; Zhao, Q.; Huang, D.; Han, J.; Su, G.; Ge, D.; Hou, Z. Tumor-Specific Endogenous FeII-Activated, MRI-Guided Self-Targeting Gadolinium-Coordinated Theranostic Nanoplatforms for Amplification of ROS and Enhanced Chemodynamic Chemotherapy. *ACS Appl. Mater. Interfaces* **2020**, *12*, 14884–14904.
- (49) Chou, T.-C. Drug Combination Studies and Their Synergy Quantification Using the Chou-Talalay Method. *Cancer Res.* **2010**, *70*, 440–446.
- (50) Gao, W.; Sun, Y.; Cai, M.; Zhao, Y.; Cao, W.; Liu, Z.; Cui, G.; Tang, B. Copper Sulfide Nanoparticles as a Photothermal Switch for TRPV1 Signaling to Attenuate Atherosclerosis. *Nat. Commun.* **2018**, *9*, 1–10.